Axion cooling of neutron stars

Armen Sedrakian

Institute for Theoretical Physics, J. W. Goethe-University, D-60438 Frankfurt-Main, Germany
(Received 4 January 2016; published 22 March 2016)

Cooling simulations of neutron stars and their comparison with the data from thermally emitting x-ray sources put constraints on the properties of axions, and by extension, of any light pseudoscalar dark matter particles, whose existence has been postulated to solve the strong-*CP* problem of QCD. We incorporate the axion emission by pair-breaking and formation processes by *S*- and *P*-wave nucleonic condensates in a benchmark code for cooling simulations, as well as provide fit formulas for the rates of these processes. Axion cooling of neutron stars has been simulated for 24 models covering the mass range 1 to 1.8 solar masses, featuring nonaccreted iron and accreted light-element envelopes, and a range of nucleon-axion couplings. The models are based on an equation state predicting conservative physics of superdense nuclear matter that does not allow for the onset of fast cooling processes induced by phase transitions to non-nucleonic forms of matter or high proton concentration. The cooling tracks in the temperature vs age plane were confronted with the (time-averaged) measured surface temperature of the central compact object in the Cas A supernova remnant as well as surface temperatures of three nearby middle-aged thermally emitting pulsars. We find that the axion coupling is limited to $f_a/10^7$ GeV $\geq$ (5–10), which translates into an upper bound on axion mass $m_a \leq (0.06$–$0.12)$ eV for Peccei-Quinn charges of the neutron $|C_n| \sim 0.04$ and proton $|C_p| \sim 0.4$ characteristic for hadronic models of axions.

I. INTRODUCTION

Astrophysics provides means for constraining properties of dark matter particles—in particular, light pseudoscalar particles such as *axions* [1,2]. Axions were originally introduced in the context of the Peccei-Quinn mechanism, which postulates a new global $U(1)_{PQ}$ symmetry [3,4] to solve the strong-*CP* problem in QCD [5], but they may play a significant role in cosmology and in stellar physics. Stellar physics of the Sun and solar-type stars, red giants, white dwarfs and supernovae puts constraints on the couplings of axions to standard-model (SM) particles [6]. The constraints are set by requiring that the coupling of axions to SM particles not alter significantly the agreement between theoretical models and observations. Axions may efficiently be produced in the interiors of stars and act as an additional sink of energy; therefore, they can alter the energetics of some processes—for example, a type-II supernova explosion. Several authors noted that the emission of axions (*a*) in the nucleon (*N*) bremsstrahlung $N + N \rightarrow N + N + a$ may drain too much energy from the type-II supernova process, making it energetically inconsistent with observations of such events [7–11]. Axions will not affect the neutrino burst if they are trapped inside the newborn neutron star, which would be the case if the axion mass is larger than 10^{-2} eV [9]. In this case the axions are radiated, in analogy to neutrinos, from the "axion sphere." Combined studies of the free-streaming and trapping regimes suggest that an axion with mass in the interval 10^{-3} to 2 eV is excluded by the observation of neutrinos from SN 1987A [9]. The coupling of axions to other SM particles is also constrained by stellar physics. For example, the axion coupling to electrons is constrained by the cooling of white dwarfs and red giants, where the underlying energy-loss mechanism is the axion emission by bremsstrahlung of electrons scattering off nuclei [12–15]. Solar physics provides another example where energy arguments allow us to place limits on beyond-SM physics; see Refs. [16,17]. These stellar constraints are complemented by experimental [18] and cosmological [19] bounds. For reviews of astrophysical limits on axion properties, see Refs. [20,21].

Neutron star cooling by neutrino emission is a highly sensitive tool to study the interior composition of neutron stars (see, for example, reviews [22–24]). Neutron star cooling via axions has evaded detailed scrutiny, although a number of key reactions necessary for such an analysis have been computed long ago [25–28] (for details, see Sec. II B). Umeda *et al.* [29], in their pioneering study of axion cooling of neutron stars, considered the axion radiation process via the bremsstrahlung in *NN* collisions in bulk nuclear matter. However, neutrino-antineutrion pair emission via Cooper pair-breaking-formation (PBF) processes [30,31], which start to operate below the critical temperature of transition of baryons to the superfluid state, plays an important role in the modern simulations of cooling of neutron stars. These processes act as the dominant cooling agent during the *neutrino cooling era* (i.e., the time span $0.1 \leq t \leq 100$ kyr) if the fast cooling processes are not operative. Previously, Ref. [32] (hereafter abbreviated as KS) computed the axion counterparts of the PBF processes in neutron stars and set approximate limits

065044-1

on the axion's coupling to baryons and its mass by requiring that the axion emission rate via the PBF processes be smaller than its neutrino counterpart [33–37].

The purpose of this work is to continue the KS analysis by incorporating the rates of the PBF processes in a cooling simulation code. Here we compute a large sample of cooling models of neutron stars and confront them with observations. The first aspect of our strategy is to use a *conservative model* of cooling which is not contaminated by the uncertainties in the rates of rapid neutrino emission processes, which in turn strongly depend on the composition of dense matter at densities above the saturation of nuclear matter. Modern simulations of the cooling of neutron stars (see, for example, the work by different groups on hadronic models [38–43] and hybrid star models [44–47]) demonstrate that fast neutrino processes do not operate in low-mass neutron stars with $M \leq 1.5 M_{\odot}$, because each such process is associated with a certain density threshold (which need not be sharp; see in particular Refs. [40,41] for this type of modeling). Light neutron stars may not achieve these thresholds in their centers, and therefore they will follow the *slow cooling* scenario which is in line with the *minimal cooling paradigm* that excludes fast cooling processes *per se* [38]. Below, the axion bounds will be derived from simulations of the cooling of low-mass stars. (We will also report results obtained for more massive stars in the framework of minimal cooling, i.e., by simply excluding the fast processes, such as the direct Urca process.) The Akmal-Pandharipande-Ravenhall (APR) equation of state (EOS) that will be used in our simulations has nucleons and leptons as constituents of matter at all densities and does not include non-nucleonic degrees of freedom [38].

The second aspect of our strategy is to concentrate on a small sample of relatively high-temperature young and intermediate-aged objects which reside within the time domain $0.1 \leq t \leq 100$ kyr and which are known to be weakly magnetized. The latter choice guarantees that no contamination will arise from the uncertain physics of internal heating processes. As argued in KS, a single example that does not fit into the axion cooling scenario already constrains the coupling of axions to SM particles. As a representative for young nonmagnetized neutron stars we choose the compact central object (CCO) located in the Cas A supernova remnant. As with all CCOs, this neutron star emits radiation in x rays without counterparts at other wavelengths. As a representative for intermediate-aged neutron stars, we selected three nearby thermally emitting neutron stars, two of which are radio-active pulsars B0656 + 14 and B1055-52, with the third being the radio-quiet neutron star Geminga.

Finally, we use a benchmark code [48] which incorporates standard microphysical input (EOS, gaps, etc.) used commonly in the cooling simulations. For details of the code, physics input and results, see Ref. [38] and references

therein. We also conducted simulations with an alternative code described in Refs. [44–46], with different EOSs and microphysics input, and obtained quantitatively good agreement at the relevant intermediate- and late-time cooling.

This paper is structured as follows: In Sec. II we review the axion properties and their emission rates in neutron stars. The cooling simulations and the results are discussed in Sec. III. Our conclusions and an outlook are given in Sec. IV.

II. AXION EMISSION RATES IN NEUTRON STARS

A. Axion couplings to SM particles

Quantum chromodynamics (QCD), the fundamental theory of strong interactions, violates the combined *CP* symmetry due to a topological interaction term in the QCD Lagrangian

$$\mathcal{L}_{\theta} = \frac{g^2 \theta}{32\pi^2} F^a_{\mu\nu} \tilde{F}^{\mu\nu a}, \qquad (1)$$

where $F^a_{\mu\nu} = \partial_\mu A_\nu - \partial_\nu A_\mu + g f^{abc} A_{\mu b} A_{\nu c}$ is the gluon field strength tensor, g is the strong coupling constant, $\tilde{F}^a_{\mu\nu} = \epsilon_{\mu\nu\lambda\rho} F^{\lambda\rho a}/2$, f^{abc} are the structure constants of the $SU(3)$ group, and the parameter θ, which is periodic with period 2π, parametrizes the nonperturbative vacuum states of QCD $|\theta\rangle = \sum_n \exp(-in\theta)|n\rangle$; here n is the winding number characterizing each distinct state, which is not connected to another by any gauge transformation [5]. If quarks are present, then the physical parameter is $\bar{\theta} = \theta + \arg \det m_q$, where m_q is the matrix of quark masses. Experimentally, the upper bound on the value of this parameter is $\bar{\theta} \lesssim 10^{-10}$, which is based on the measurements of the electric dipole moment of the neutron, $d_n < 6.3 \times 10^{-26} e$ cm [49]. SM does not provide an explanation on why $\bar{\theta}$ is not of the order of unity—a fact known as the strong *CP* problem.

The Peccei-Quinn mechanism solves the *CP* problem by introducing an new global $U(1)_{PQ}$ symmetry which adds an additional anomaly term to the QCD action proportional to the axion field a [1,3]. The axion field value is then given by $\langle a \rangle \sim -\bar{\theta}$. The physical axion field is then $a - \langle a \rangle$, and the undesirable θ term in the action is replaced by the physical axion field, which can be viewed as the Nambu-Goldstone boson of the Peccei-Quinn $U(1)_{PQ}$ symmetry breaking [1,2].

The Lagrangian of axion field a has the form

$$\mathcal{L}_a = -\frac{1}{2} \partial_\mu a \partial^\mu a + \mathcal{L}^{(N)}_{\text{int}}(\partial_\mu a, \psi_N) + \mathcal{L}^{(L)}_{\text{int}}(a, \psi_L), \quad (2)$$

where the second term describes the coupling of the axion to nucleon fields (ψ_N) and the third term describes the coupling to the lepton fields (ψ_L) of the SM. The coupling of axion to nucleonic fields is described by the following interaction Lagrangian:

$$\mathcal{L}_{\text{int}}^{(B)} = \frac{1}{f_a} B^\mu A_\mu, \tag{3}$$

where f_a is the axion decay constant, and the baryon and axion currents are given by

$$B^\mu = \sum_N \frac{C_N}{2} \bar{\psi}_N \gamma^\mu \gamma_5 \psi_N, \qquad A_\mu = \partial_\mu a, \tag{4}$$

where $N \in n, p$ labels neutrons and protons, and C_N are the Peccei-Quinn (PQ) charges of the baryonic currents. The dimensionless Yukawa coupling can be defined as $g_{aNN} = C_N m_N / f_a$ with the implied "fine-structure" constant $\alpha_{aNN} = g_{aNN}^2 / 4\pi$. The coupling of axions to leptons (in practice we consider only electrons) is commonly taken in the pseudoscalar form

$$\mathcal{L}_{\text{int}}^{(e)}(a, \psi_e) = -i g_{aee} \bar{\psi}_e \gamma_5 \psi_e a, \tag{5}$$

where the Yukawa coupling is given by $g_{aee} = C_e m_e / f_a$. The C_N charges are generally given by generalized Goldberger-Treiman relations:

$$C_p = (C_u - \eta)\Delta_u + (C_d - \eta z)\Delta_d + (C_s - \eta w)\Delta_s, \tag{6}$$

$$C_n = (C_u - \eta)\Delta_d + (C_d - \eta z)\Delta_u + (C_s - \eta w)\Delta_s, \tag{7}$$

where $\eta = (1 + z + w)^{-1}$, with $z = m_u/m_d$, $w = m_u/m_s$, and $\Delta_u = 0.84 \pm 0.02$, $\Delta_d = -0.43 \pm 0.02$ and $\Delta_s = -0.09 \pm 0.02$. The main uncertainty is associated with $z = m_u/m_d = 0.35$–0.6. For *hadronic axions*, $C_{u,d,s} = 0$, and the nucleonic charges vary in the range

$$-0.51 \leq C_p \leq -0.36, \qquad -0.05 \leq C_n \leq 0.1. \tag{8}$$

These ranges imply that neutrons may not couple to axions ($C_n = 0$), whereas protons always couple to axions $C_p \neq 0$. The values of PQ charges define a continuum of axion models; for a review see, for example, Ref. [4]. In the so-called *invisible axion* DFSZ model, these couplings are of the same order of magnitude and are related via the ratio of two Higgs vacuum expectation values $\tan\beta$ as follows: $C_e = \cos^2\beta/3$, $C_u = \sin^2\beta/3$, $C_d = \cos^2\beta/3$, where β is a free parameter. In the alternative KVSZ model, ordinary SM particles do not have PQ charges and $C_e = 0$; the coupling of baryons to axions arises from PQ charges of unknown very heavy quarks. To keep the discussion general enough, we will abstract from a particular axion model and will treat the PQ charges of fermions as free parameters taken from the range (8); we will also explore the case of large neutron PQ charge to contrast our result with the case where $|C_n| \sim |C_p|$. If only nucleonic processes are considered, the emission rates depend on a certain combination of charges and axion decay constant.

In general, when leptonic processes are involved, this is not the case.

The axion mass is related to f_a via the relation

$$m_a = \frac{z^{1/2}}{1 + z} \frac{f_\pi m_\pi}{f_a} = \frac{0.6 \text{ eV}}{f_a/10^7 \text{ GeV}}, \tag{9}$$

where the pion mass $m_\pi = 135$ MeV, decay constant $f_\pi = 92$ MeV, and we adopt from the range of z values quoted the value $z = 0.56$. Equation (9) translates a lower bound on f_a into an upper bound on the axion mass.

B. Axion emission via PBF process

KS obtained the axion emissivity of S-wave paired superfluid by assuming that the PQ charges of nucleons are fixed by $C_N/2 = 1$. By matching Eq. (5) of KS with Eq. (4), we see that we need to rescale their $f_a^{-1} \to (C_N/2)f_a^{-1}$ to obtain explicitly the expression for the axion emissivity in the present notations. Thus, the axion emissivity now reads

$$\epsilon_{aN}^S = \frac{2C_N^2}{3\pi} f_a^{-2} \nu_N(0) v_{FN}^2 T^5 I_{aN}^S, \tag{10}$$

where $\nu_N(0) = m_N^* p_{FN}/\pi^2$ is the density of states at the Fermi surface, v_{FN} is the Fermi velocity, the superscript S indicates isotropic pairing in the $^1S_0$ channel,

$$I_{aN}^S = z_N^5 \int_1^\infty dy \frac{y^3}{\sqrt{y^2 - 1}} f_F(z_N y)^2, \tag{11}$$

and $z_N = \Delta_N^S(T)/T$. The bound obtained by KS from the requirement that the axion cooling not overshadows the cooling via neutrinos after rescaling reads

$$\frac{\epsilon_a^S}{\epsilon_\nu^S} = \frac{59.2 C_N^2}{4 f_a^2 G_F^2 \Delta_N^S(T)^2} r(z) \leq 1, \tag{12}$$

where $r(z)$ is the ratio of the phase-space integral for axions (11) and its counterpart for neutrinos and is numerically bound from above $r(z) \leq 1$; therefore it can be dropped from the bound on f_a. Substituting the value of the Fermi coupling constant $G_F = 1.166 \times 10^{-5}$ GeV^{-2} in Eq. (12), we rewrite the bound found by KS as

$$\frac{f_a/10^{10} \text{ GeV}}{C_N} > 0.038 \left[\frac{1 \text{ MeV}}{\Delta^S(T)}\right], \tag{13}$$

which now includes the PQ charge of the neutron or proton explicitly. Using Eq. (9), this translates to an upper bound on the axion mass of

$$m_a C_N \leq 0.163 \text{ eV} \left(\frac{\Delta_N^S(T)}{1 \text{ MeV}}\right). \tag{14}$$

Note that the nucleon pairing gap on the right-hand side can be replaced by the critical temperature T_c, because in the range of temperatures important for pair-breaking processes, $0.5 \leq T/T_c < 1$, the BCS theory predicts $\Delta(T) \simeq T_c$.

Neutron condensate in neutron star cores is paired in the $^3P_2$-$^3F_2$ channel in a state which features an anisotropic gap [50]. As pointed out in KS, the results above can be trivially extended to the P-wave pairing following analogous discussion for neutrino emission in Ref. [33]. The corresponding axion emissivity is obtained from the S-wave rate above (10) by setting $v_{Fn}^2 = 1$ and angle-averaging the phase-space integral (11) to account for the anisotropy of the gap

$$\epsilon_{an}^P = \frac{2C_n^2}{3\pi} f_a^{-2} \nu_n(0) T^5 I_{an}^P, \quad (15)$$

where

$$I_{an}^P = \int \frac{d\Omega}{4\pi} z_N^5 \int_1^\infty dy \frac{y^3}{\sqrt{y^2 - 1}} f_F(z_N y)^2, \quad (16)$$

where $d\Omega$ denotes the integration over the solid angle and $z_N = \Delta^P(T, \theta)/T$ depends on the polar angle θ, where $\Delta^P(T, \theta)$ is the pairing gap in the P-wave channel. By adapting Eq. (11) to the P-wave case, we automatically include the vertex corrections that were omitted in Ref. [33]. Note that $C_n = 0$ is not excluded; i.e., conceivably axions may not be emitted by the neutron P-wave condensate.

For the purpose of numerical simulations of axion cooling, it is useful to obtain fits to the dependence of the integrals (11) and (16) on reduced temperature $\tau = T/T_c$, where T_c is the critical temperature. We first obtain the asymptotic forms of these integrals in the limits $T \to 0$ and $T \to T_c$. In the low-temperature limit $\Delta(T)/T \gg 1$, i.e., $z \gg 1$, and because $y \geq 1$ we can set in (11) $f_F^2(zy) = \exp(-2yz)$. (We drop the indices N, n and p in the intermediate steps and recover them in the final expressions). The integration with subsequent expansion in $z \gg 1$ gives

$$I_{aN}^S = z^5 \left[K_1(2z) + \frac{K_2(2z)}{2z} \right] \simeq \frac{z^5}{2} \sqrt{\frac{\pi}{z}} \exp(-2z), \quad (17)$$

where $K_n(z)$ is the Bessel function of the second kind of nth order.

In the limit $T \to T_c$, we approximate the denominator of the integrand $\sqrt{y^2 - 1} \simeq y$ and obtain

$$I_{aN}^S = (9\zeta(3) - \pi^2) \frac{\Delta_N^2}{6T^2} \simeq 0.158 \frac{\Delta_N^2}{T^2}. \quad (18)$$

There exist two competing states for P-wave superfluid, which differ by the anisotropy of the gap. We denote these

states as A and B and assign them the following dependences on the angle θ:

$$\Delta^A = \Delta_0^A \sqrt{1 + 3\cos^2\theta}, \qquad \Delta^B = \Delta_0^B \sin\theta. \quad (19)$$

In the high-temperature ($T \to T_c$) limit, we have

$$I_{an}^{P^A} = I_{an}^P \int \frac{d\Omega}{4\pi} (1 + 3\cos^2\theta) = 2I_{an}^{P^0}, \quad (20)$$

$$I_{an}^{P^B} = I_{an}^P \int \frac{d\Omega}{4\pi} \sin^2\theta = \frac{2}{3} I_{an}^{P^0}, \quad (21)$$

where $I_{an}^{P^0}$ stands for the isotropic part of the integral and is given by (18) where Δ_N is replaced by $\Delta_0^{A,B}$. In the anisotropic case, the low-temperature limit does not have a simple analytical representation.

The exact numerical calculations of the integrals (11) and (16) were fitted in the range $0 \leq z \leq 15$ using suitable functions which reproduce correct asymptotic forms as described above. For S-wave pairing, we used the following fit formula:

$$I_{aN}^S(z) = (az^2 + cz^4)\sqrt{1 + fz}\, e^{-\sqrt{4z^2 + h^2} + h}, \quad (22)$$

where $a = 0.158151$, $c = 0.543166$, $h = 0.0535359$, and $f = \pi/4c^2$. This formula fits the numerical result with relative accuracy $\leq 5.6\%$ for $z \sim 1$ and much more accurately in the asymptotic regimes. In the case of P^A-wave pairing, we used the function

$$I_{an}^{P^A}(z) = \frac{(az^2 + cz^4)(1 + fz^2)}{(1 + bz^2 + gz^4)} e^{-\sqrt{4z^2 + h^2} + h}, \quad (23)$$

where $a = 2 \times 0.158151$, $b = 0.856577$, $c = 0.0255728$, $f = 2.22858$, $g = 0.000449543$ and $h = 2.22569$. The relative accuracy of the fit is $\leq 4\%$ at $z \sim 10$ and is better in the rest of the domain. Finally, in the case of P^B-wave pairing we used the function

$$I_{an}^{P^B}(z) = \frac{(az^2 + cz^4)\sqrt{1 + fz^2}}{(1 + bz^2 + gz^4)}, \quad (24)$$

where $a = (2/3) \times 0.158151$, $b = -0.043745$, $c = -0.000271463$, $f = 0.0063470221$, $g = 0.0216661$. The relative error in this case remains below 2%. The exact results for the integrals (11) and (16) are shown in Fig. 1 together with the approximate fits given by Eqs. (22)–(24).

C. Axion bremsstrahlung emission in the crust

Electrons undergoing acceleration in the vicinity of a nucleus characterized by charge Z and mass number A will emit axions. The PQ charge of electrons C_e is related to the dimensionless coupling of axions to electrons by
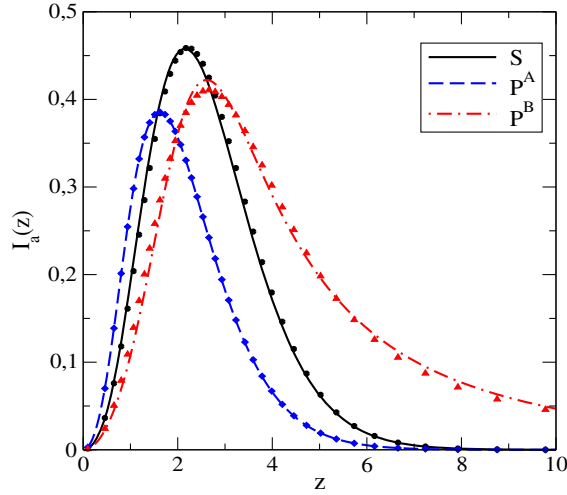
FIG. 1. Dependence of the integrals (11) and (16) on $z = \Delta(T)/T$. The exact results are shown by symbols, whereas the fits are shown by lines.

$g_{aee} = C_e m_e / f_a$. The emissivity of the axion bremsstrahlung process is given by [25,27]

$$\epsilon_{aee} = \frac{\pi^2}{120} \frac{Z^2 \alpha}{A} \left(\frac{C_e m_e}{f_a \epsilon_e} \right)^2 n_B T^4 \left[2 \ln(2\gamma) - \ln \frac{\alpha}{\pi} \right], \quad (25)$$

where ϵ_e is the Fermi energy of electrons and γ is the Lorentz factor of ultrarelativistic electrons, $\alpha = 1/137$ is the fine-structure constant, and n_B is the baryon number density. This axion bremsstrahlung process has its neutrino-pair emission counterpart, and its rate is given by [51]

$$\epsilon_{\nu ee} = \frac{8\pi}{567} G_F^2 C_+^2 Z^2 \alpha^4 n_i T^6 L, \quad (26)$$

where $C_+^2 = 1.675$, $0 \leq L \leq 1$ includes many-body corrections to the rate of the process related to the correlations among the nuclei, electron screening, finite nuclear size, etc., and n_i is the number density of nuclei. To see the relative importance of the axion and neutron emissivities, we fix the electron PQ charge $C_e = 1$, in which case the ratio of the axion to neutrino emissivity is given by

$$\frac{\epsilon_{aee}}{\epsilon_{\nu ee}} \simeq \frac{189\pi}{320} \frac{C_e^2}{(C_+ G_F T f_a)^2 \alpha^3 L} \left(\frac{m_e}{\epsilon_e} \right)^2$$

$$= 2.8 \left(\frac{1}{T/10^9 \text{ K}} \right)^2 \left(\frac{1}{f_a/10^{10} \text{ GeV}} \right)^2, \quad (27)$$

where for the sake of estimate we set $m_e/\epsilon_e = 10^{-2}$, $L = 1$ and set the expression in brackets in Eq. (25) equal to unity. We also use $n_B/A = n_i$, which applies when the density of free neutrons in the crust is negligible, as has been assumed in Eq. (8) of Ref. [25].

D. Axion bremsstrahlung emission in the core

To describe the axion emission in the core of the neutron stars, we consider the processes involving neutrons, protons and electrons; the EOS chosen for numerical simulations is purely nucleonic for all relevant densities, and there is no need to consider other degrees of freedom, such as hyperons or quarks. Axions will be emitted in the nucleon collisions via bremsstrahlung process (irrespective of the pairing of nucleons). The emissivity of the process $N + N \rightarrow N + N + a$, $N \in n$ or p, is given by [25,26]

$$\epsilon_{aN} = \frac{31}{945} \alpha_{aNN} \left(\frac{f_\pi}{m_\pi} \right)^4 m_N^2 p_{FN} T^6 F \left(\frac{m_\pi}{2p_{FN}} \right) \mathcal{R}, \quad (28)$$

where α_{aN} is the axion fine-structure constant (see Sec. II A), $F(x) \equiv 1 - (3/2)x \arctan(1/x) + x^2/2(1 + x^2)$. We do not reproduce the expression for the $n + p \rightarrow n + p + a$ reaction, which is more complicated due to two different Fermi surfaces involved, see Eq. (2.13) of Ref. [26]. The factor $\mathcal{R}$ stands for reduction of the axion emissivity by the superfluidity of nucleons, and we have implemented the same factors as has been done for the neutrino bremsstrahlung in the code. (For discussion, see Ref. [52].) The emissivity (28) should be viewed as an upper limit because of the approximate treatment of the nuclear interaction in the $N - N$ collisions which only include the one-pion exchange contribution to the nuclear scattering [hence the proportionality of ϵ_{aNN} to $(f_\pi/m_\pi)^4$]. The inclusion of other (repulsive) channels of interaction reduces the rate by a factor of 0.2. This argument applies also to the neutrino-pair bremsstrahlung process in nuclear collisions; therefore the relative importance of these processes in cooling neutron stars is unaffected (i.e., the ratio of the axion and neutrino emissivities is independent of the nuclear matrix element, which can be factorized if the radiation is soft).

III. COOLING SIMULATIONS

We recall that the specific purpose of this work is to (a) consider a conservative model of neutron stars without fast cooling agents which is almost certainly guaranteed for light- to medium-mass neutron stars; (b) choose observational data which are not potentially contaminated by the heating by strong magnetic fields at intermediate stages of cooling and other sources at late times; and (c) use a well-tested code with standard EOS input in order to benchmark the axion cooling of neutron stars and render the results easily reproducible.

A. Physics input

The cooling code solves the energy balance and transport equation, which can be reduced to a parabolic differential equation for the temperature of the core. The transport in the low-density blanket of the star comprising matter below the density $\rho_b = 10^{10}$ g cm^{-3} is decoupled from evolution

and is treated separately in terms of a relation between temperature at its base T and the surface of the star T_s. This relation has the generic form $T_s^4 = g_s h(T)$, where g_s is the surface gravity, and h is some function which depends on T, the opacity of crustal material, and its equation of state. The amount of the light material in the envelope is regulated by the parameter η, which takes on the value $\eta = 0$ for a purely iron surface and $\eta \to 1$ for a light-element surface. For a detailed discussion of the input physics, the reader is referred to Ref. [38] and references therein.

After the initial nonisothermal phase, the models settle into an equilibrium state which is characterized by an isothermal core and gradient-featuring envelope. In this case, the time evolution is characterized by the ordinary differential equation

$$C_V \frac{dT}{dt} = -L_\nu(T) - L_a(T) - L_\gamma(T_s) + H(T), \quad (29)$$

where L_ν and L_a are the neutrino and axion luminosities from the bulk of the star (recall that the neutrino and axion mean free paths are larger than the star radius) and L_γ is the luminosity of photons radiated from the star's surface. Here C_V is the specific heat of the core, and $H(t)$ accounts for heating processes, which could be important in the late-time evolution of neutron stars. We assume below that $H(T) = 0$ in the neutrino cooling era. The photon luminosity is given simply by the Stefan-Boltzmann law $L_\gamma = 4\pi\sigma R^2 T_s^4$, where σ is the Stefan-Boltzmann constant, and R is the radius of the star.

We have computed 24 models of cooling neutron stars by choosing three different masses $m = 1.0, 1.4, 1.8$, where m is the object mass normalized to the solar mass, light-element $\eta = 1$ and iron $\eta = 0$ envelopes, as well as four values of the axion decay constant $f_{a7} = \infty, 10, 5, 2$, where we use the units of $f_{a7} = f_a/10^7$ GeV. Throughout most of the computation, the PQ charges of neutrons and protons were fixed at $|C_n| = 0.04$ and $|C_p| = 0.4$, which reflect the asymmetry in the couplings of neutrons and protons to axions according to Eq. (8). Note that these quantities enter the axion emission rate in the combination $(f_a^*)^{-1} = (C_N/2)f_a^{-1}$; therefore cooling simulations put constraints on f_a^* rather than on f_a and C_N separately. From now on, we will also assume that $C_e = 0$—a conservative assumption which allows us to focus on PBF processes. We will return to the role of electrons in a separate study. All simulations employ the APR EOS with only nucleonic degrees of freedom, which guarantees that fast cooling processes do not act. Before presenting the results, we turn to the observational data.

B. Selecting objects

As argued previously in KS, it is sufficient to carry out fits to selected objects rather than a global fit to the population of all known thermally emitting neutron stars.

Here we use a handful of objects to mark up the early ~ 0.1 kyr and intermediate ~ 100 kyr evolution of neutron stars. For the early stages, excellent candidates are the CCOs in supernova remnants (SNRs), which comprise a family of around ten pointlike, thermally emitting x-ray sources located close to the geometrical centers of non-plerionic SNRs [53]. They do not show counterparts at any other wavelength than x rays and have low magnetic fields, which exclude heating processes at this stage of evolution.

As a *representative* for CCOs we take the *CXO J*232327.9 + 584842 in Cassiopea A SNR. It has received much attention because of its putative transient cooling claimed to occur during the past ten years. In the current context these variations are irrelevant, and we shall adopt a constant temperature $T = 2.0 \pm 0.18 \times 10^6$ K at the age 320 yr [54]. As *representatives* for late time-cooling we choose a group of three neutron stars which form a class of nearby objects that allows spectral fits to their x-ray emission [55]. Typically the spectra do not allow a single-component blackbody fit, but two-component fits are sufficient. The first object is *PSR B*0656 + 14, which is a rotation-powered pulsar. The two inferred temperatures for this object are $T_w = (6.5 \pm 0.1) \times 10^5$ K and $T_h = (1.25 \pm 0.03) \times 10^6$ K. The characteristic age of this pulsar is 1.1×10^5 yr. The second object is *PSR B1055-52*, which is again a rotation-powered pulsar [55]. The two blackbody temperature fits give $T_w = 7.9 \pm 0.3 \times 10^5$ K and $T_h = (1.79 \pm 0.06) \times 10^6$ K. The characteristic age of this pulsar is 5.37×10^5 yr. The third object is *Geminga*, which is a radio-quiet nearby x-ray-emitting neutron star [55]. The two-blackbody temperature fit gives $T_w = 5.0 \pm 0.1 \times 10^5$ K and $T_h = (1.9 \pm 0.3) \times 10^6$ K. The characteristic age of Geminga is 3.4×10^5 yr. In confronting the neutron stars' blackbody temperatures with the theoretical models, we will adopt the lower of the two values inferred. The ages of these three neutron stars are known only on the basis of a spin-down model, which is uncertain. We quantify this uncertainty by assigning a factor of 3 error to the spin-down age of each of these objects. The data on PSR B1055-52 are marginally (in)consistent with the cooling curves we find, but the uncertainties in the physics of cooling tolerate such discrepancy: first, in contrast to CCO in Cas A, only the spin-down age is known, which can have larger error than we assumed; second, at the later stages of thermal evolution, heating processes (even for weakly magnetized stars) can become a factor. Finally, the discrepancy may lie in the modeling of the pairing gaps, which can be tuned to fit the inferred temperature of PSR B1055-52.

C. Results of simulations

The results of extensive simulations are summarized in Fig. 2, where we show cooling tracks for 16 models of light- and intermediate- ($m = 1$ and $m = 1.4$) mass neutron stars for cases of a nonaccreted iron envelope ($\eta = 0$) and a light-element envelope ($\eta = 1$). For each of these cases the
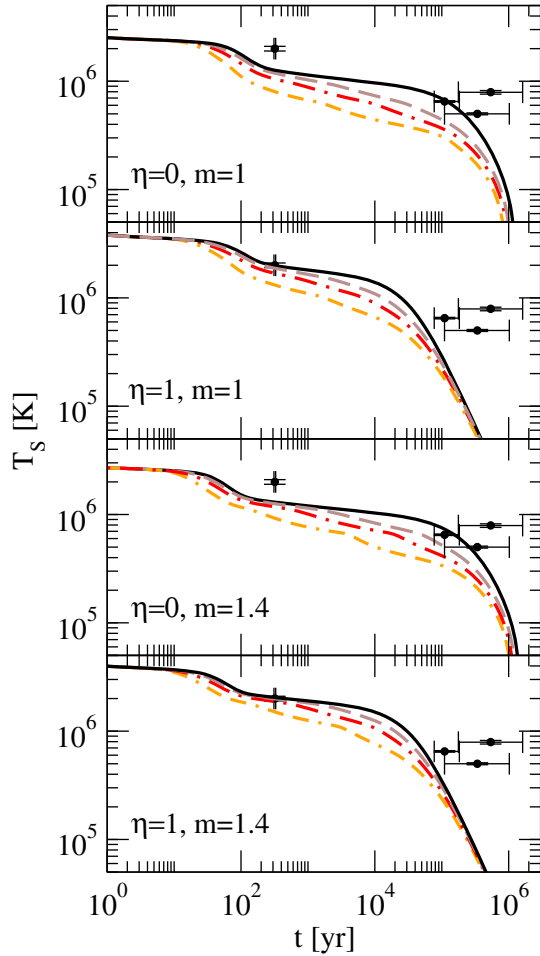
FIG. 2. Cooling tracks (*redshifted* surface temperature vs age) for neutron star models with masses $m = 1$ and $m = 1.4$ (in solar units) for the cases of nonaccreted iron envelope ($\eta = 0$) and accreted light-element envelope ($\eta = 1$). The representative observational data includes (from left to right) the CCO in Cas A, PSR B0656 + 14, Geminga, and PSR B1055-52. Each panel contains cooling tracks for various values of the axion coupling constant; the case $f_a = \infty$ (solid line) corresponds to vanishing axion coupling—i.e., purely neutrino cooling. The axion cooling models are shown for the values $f_{a7} = 10$ (dashed), $f_{a7} = 5$ (dash-dotted), and $f_{a7} = 2$ (double-dash-dotted).

axion coupling has been assigned the following values: $f_a = \infty$ (negligible coupling), $f_{a7} = 10$, $f_{a7} = 5$ and $f_{a7} = 2$, where $f_{a7} = f_a/10^7$ GeV, in combination with charges $|C_n| = 0.04$ and $|C_p| = 0.4$.

The observational temperatures of the four objects discussed are shown by dots with error bars. The temperature of CCO in Cas A is consistent with the cooling of $m = 1$ and 1.4 mass stars assuming that the compact object in Cas A has a light-element envelope and axion cooling is absent. Switching on the axion cooling decreases the temperatures of models with the age of CCO in Cas A because of the additional losses caused by the axion PBF process. It is seen that for small enough values of f_a, the cooling curves become inconsistent with the Cas A data.
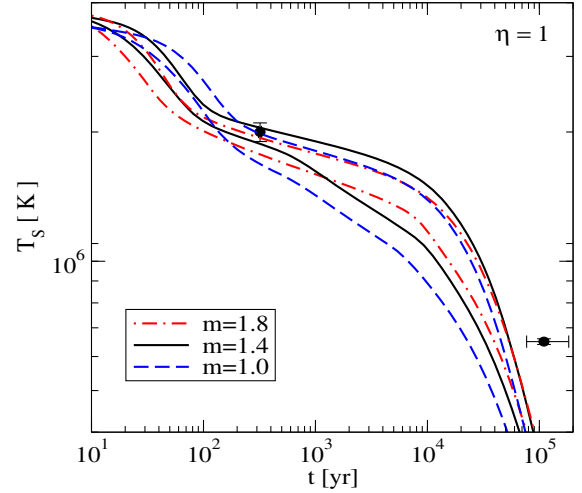

FIG. 3. Cooling tracks of neutron star models with masses $m = 1$ (dash-dotted) 1.4 (solid) and 1.8 (dashed) for the case of an accreted light-element envelope ($\eta = 1$) along with the measured temperature of CCO in Cas A. For each value of mass, the upper curve corresponds to the cooling without axions, and the lower curve corresponds to axion cooling with $f_{a7} = 5$. Note the weak dependence on the surface temperature of models on the star mass.

Quantitatively, the lowest value of axion coupling $f_{a7} = 2$ is inconsistent with both $m = 1$ and $m = 1.4$ mass cooling; the value $f_{a7} = 5$ is inconsistent with $m = 1$ but not with $m = 1.4$ mass star cooling.

The temperatures of the remaining middle-aged neutron stars from our collection are consistent with the cooling of $m = 1$ and 1.4 mass star models if we make the natural assumption that these neutron stars have nonaccreted iron envelopes. Axion cooling with $f_{a7} \leq 5$ is clearly inconsistent with the data on these objects. For $f_{a7} = 10$ and $m = 1.4$, the cooling tracks are marginally consistent with the data. Physically, the inconsistency arises from the PBF axion cooling of the models *prior* to the actual age of these objects, which according to simulations are currently cooling predominantly via crust bremsstrahlung and surface photon emission.

Figure 3 focuses on the cooling behaviour at the early stages of evolution and on CCO in Cas A. Here we have added also cooling tracks for massive $m = 1.8$ stars to quantify the variations in the mass of the objects. It is seen that significant variations in the mass do not change the cooling tracks; this would, of course, change if the EoS of dense matter admits fast cooling processes—i.e., if in more massive stars the threshold densities for the onset of rapid cooling processes are attained. Our computations show that $f_{a7} = 10$ cooling is still consistent with the data for $m = 1.4$ stars, but for $f_{a7} = 5$ cooling tracks are inconsistent with the data independent of the mass of the star, as shown in Fig. 3.

Figure 4 focuses on the cooling of the three intermediate-aged neutron stars discussed above with and without axion cooling. The variation in the mass range $1 \leq m \leq 1.8$ does
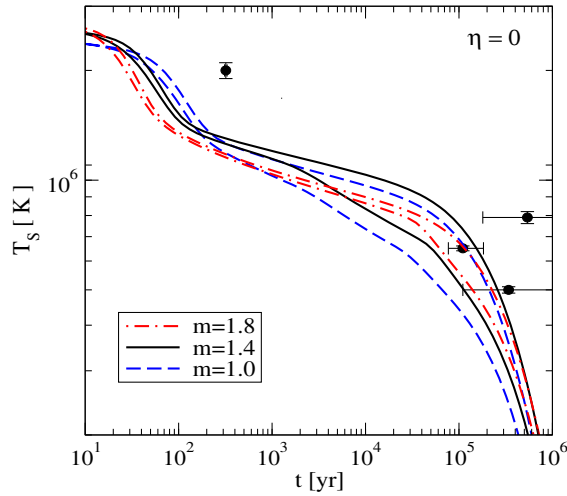
FIG. 4.   Cooling tracks of neutron star models with masses $m = 1$ (dashed) 1.4 (solid), and 1.8 (dash-dotted) for the case of a nonaccreted iron envelope ($\eta = 0$). The measured temperatures of PSR B0656 + 14, Geminga are consistent with neutrino cooling tracks; the uncertainty in the spin-down age of PSR B1055-52 and internal heating may account for marginal inconsistency. The axion cooling tracks are shown for $f_{a7} = 10$.

not induce significant changes in the cooling tracks, provided that fast cooling processes do not operate in the massive $m = 1.8$ model. The data are consistent with neutrino-only cooling, assuming that some minor adjustment can improve the agreement with PSR B1055-52 data. (We recall that the spin-down age may have larger error than assumed, or some heating processes may already operate in this object.) Turning on the axion cooling, it is seen that $f_{a7} = 10$ cooling tracks are clearly inconsistent with the data independent of the mass of the star.

To conclude, the combination of observational data and simulations including cases with nonaccreted ($\eta = 0$) and accreted ($\eta = 1$) envelopes suggests that the range of axion coupling constant for which axion cooling is inconsistent with data lies within $5 \leq f_{a7} \leq 10$, independent of the mass of the star.

So far, we have fixed the values of PQ charges of the neutron and proton to some characteristic values taken from the range defined by the inequalities (8). The proton PQ charge is constrained in this class of theories to a narrow range of values, while the neutron PQ charge changes the sign, thus allowing for zero coupling of the axion to the neutron. Furthermore, the PQ charge of neutron is at least a factor of 4 smaller than the proton charge. For the value of $|C_n| = 0.04$ we adopted and for our choice of pairing gaps, the axion emission is dominated by proton condensate, and the emission from neutron condensates is negligible. To see the possible effect of the neutron condensate on the cooling evolution, in particular on the range of the temperatures and the time span where it may play a role, we have simulated the cooling with a model where $|C_n|=|C_p|=0.4$. Figure 5 shows the cooling models in the case of
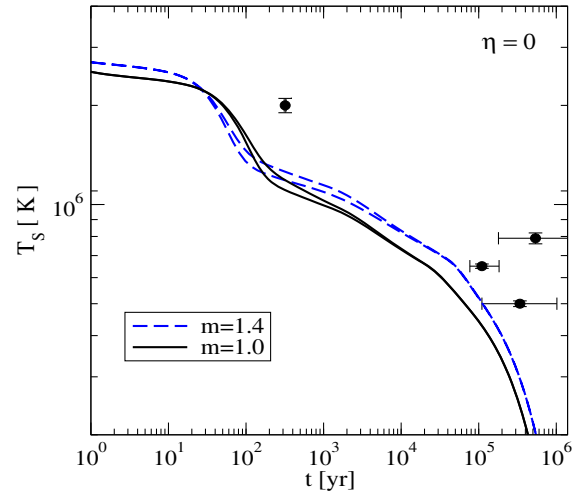

FIG. 5.   Cooling tracks of neutron star models with masses $m = 1$ (solid) and 1.4 (dashed) for the case of a nonaccreted iron envelope ($\eta = 0$) and for $f_{a7} = 10$. For each mass, the two tracks differ by the value of the neutron PQ charge. The upper curves correspond to our standard choice $|C_n| = 0.04$, while the lower curves correspond to the case of enhanced axion emission with $|C_n| = |C_p| = 0.4$.

nonaccreted envelops ($\eta = 0$) for light neutron star models and the value of axion coupling $f_{a7} = 10$. For each mass we show two cooling curves with $|C_n| = 0.04$ and $|C_n| = 0.4$ (where the upper curve always corresponds to the small value of $|C_n|$). The same, but in the case of accreted envelopes ($\eta = 1$), is shown in Fig. 6. Axion emission by neutron condensate lowers the surface temperatures of the models by a factor of the order of unity; therefore, the cases where $|C_n| \sim |C_p|$ will have qualitatively similar bounds to those obtained above. It is seen that the neutron condensate affects cooling during the time span $10^2 \leq t \leq 10^3$ yr, which corresponds to interior temperatures in the range $0.5T_c \leq T < T_c$. The role of the neutron condensate can
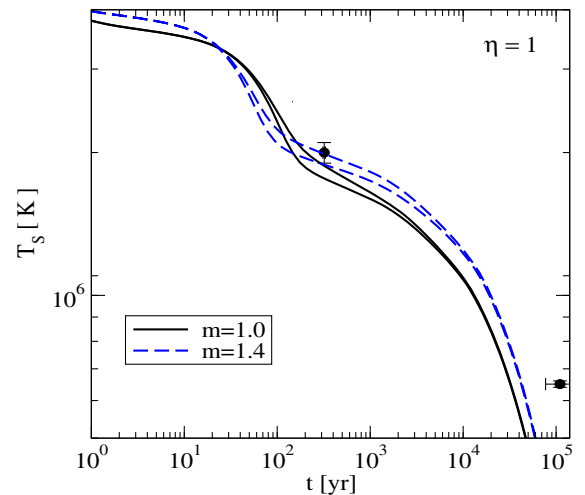

FIG. 6.   Same as in Fig. 5, but in the case of an accreted envelope ($\eta = 1$).

become important if fine-tuning of the cooling curves to data will be required, as is possibly the case for the CCO in Cas A (see Ref. [46] and references therein).

IV. DISCUSSION AND CONCLUSIONS

This work explores how the emission of axions by weakly magnetized neutron stars during their early ($t \sim 0.1$ kyr) and intermediate ($t \sim 10^2$ kyr) evolution alters their observable surface temperatures. As a benchmark, we modeled the purely neutrino cooling of neutron stars within a slow cooling scenario where any fast cooling processes, such as the direct Urca processes on nucleons and quarks, are excluded. These purely neutrino cooling models are consistent with the temperature of CCO in Cas A if we assume this object has a light-element envelope; these cooling tracks are also consistent with the older pulsars and Geminga if we assume a nonaccreted, iron envelope and account for errors in the age determinations and possible changes due to internal heating. The dependence of the cooling tracks on the mass of the models is rather weak because of absence of fast cooling agents. We further explored the influence of axion cooling bremsstrahlung processes on the cooling tracks of our models by smoothly varying the axion coupling constant f_a (the strength of the coupling scales as $1/f_a$). In doing so, we fixed the PQ charges of the neutron and proton at the values $|C_n| = 0.04$ and $|C_p| = 0.4$ motivated by hadronic models of axions [see Eq. (8)] and neglected the coupling of the axion to electrons, $C_e = 0$ (this would correspond to the KVSZ class of models of axions). The latter conservative assumption strengthens the limits, because the inclusion of axion emission by electron bremsstrahlung processes would have increased the discrepancy between the models and purely neutrino cooling models. We find that the value of $f_{a7} = 5$ is clearly inconsistent with the combined observational data, and $f_{a7} = 10$ is inconsistent with the surface temperatures of middle-aged neutron stars. Using these bounds in the relation (9), we obtain the following conservative limit on the axion mass:

$$f_a/10^7 \text{ GeV} \geq (5\text{--}10), \qquad m_a \leq (0.06\text{--}0.12) \text{ eV}, \quad (30)$$

which can be contrasted with the bound given by KS (14) for the value $C_N = |C_p| = 0.4$:

$$f_a/10^7 \text{ GeV} \geq 15.2, \qquad m_a \leq 0.04 \text{ eV}. \quad (31)$$

The obtained upper bound on the mass of the axion is consistent with those obtained from the supernova [7–11] and proton-neutron star [9] physics, $m_a \leq 0.1$ eV. However, the limit (30) is based on a rather conservative segment of physics of the cooling of neutron stars and surface temperature data measured from nearby x-ray-emitting neutron stars and is complementary to the one quoted above. The bounds derived from proto–neutron stars share the same type of uncertainties as the cold neutron star model, while the supernova limits suffer from the uncertainty in the basic mechanism that drives supernova explosions. Limits similar to ours were obtained by Umeda *et al.* [29] in their pioneering study of the axion cooling of neutron stars, although their study does not include the key PBF processes; i.e., their axion cooling is dominated by nucleon bremsstrahlung processes.

Looking ahead, it should be mentioned that the present study selected only a single pair of values of PQ charges for neutrons and protons from a range defined for hadronic models of axions. In general, these charges may vary and thus define a continuum of axion models. A broader overview of the axion cooling of neutrons can be obtained by varying independently these two parameters, as well as by fixing their values to specific models such as the DVSZ or the KVSZ models. A further point for a future study is the role of the axion bremsstrahlung by electrons. Electron bremsstrahlung of axions in the crust at later stages of neutron star cooling (which we neglected in this study assuming $C_e = 0$, as in the KVSZ model) needs to be included in the theoretical models of axion cooling. This will allow us to improve the constraints on the axion mass, as additional axion emission will lead to discrepancies between the theory and observations at larger values of f_a than quoted above.

ACKNOWLEDGMENTS

[1] F. Wilczek, Phys. Rev. Lett. **40**, 279 (1978).
[2] S. Weinberg, Phys. Rev. Lett. **40**, 223 (1978).
[3] R. D. Peccei and H. R. Quinn, Phys. Rev. Lett. **38**, 1440 (1977).
[4] R. D. Peccei, in *Axions*, edited by M. Kuster, G. Raffelt, and B. Beltrán, Lecture Notes in Physics Vol. 741 (Springer-Verlag, Berlin, 2008), pp. 3–540.
[5] G. 't Hooft, Phys. Rev. Lett. **37**, 8 (1976).

[6] G. G. Raffelt, J. Redondo, and N. V. Maira, Phys. Rev. D **84**, 103008 (2011).

[7] R. P. Brinkmann and M. S. Turner, Phys. Rev. D **38**, 2338 (1988).

[8] A. Burrows, M. S. Turner, and R. P. Brinkmann, Phys. Rev. D **39**, 1020 (1989).

[9] A. Burrows, M. T. Ressell, and M. S. Turner, Phys. Rev. D **42**, 3297 (1990).

[10] H.-T. Janka, W. Keil, G. Raffelt, and D. Seckel, Phys. Rev. Lett. **76**, 2621 (1996).

[11] C. Hanhart, D. R. Phillips, and S. Reddy, Phys. Lett. B **499**, 9 (2001).

[12] T. Altherr, E. Petitgirard, and T. del Río Gaztelurrutia, Astropart. Phys. **2**, 175 (1994).

[13] G. Raffelt and A. Weiss, Phys. Rev. D **51**, 1495 (1995).

[14] A. H. Córsico, O. G. Benvenuto, L. G. Althaus, J. Isern, and E. García-Berro, New Astron. **6**, 197 (2001).

[15] M. M. Miller Bertolami, B. E. Melendez, L. G. Althaus, and J. Isern, J. Cosmol. Astropart. Phys. 10 (2014) 069.

[16] N. Vinyoles, A. Serenelli, F. L. Villante, S. Basu, J. Redondo, and J. Isern, J. Cosmol. Astropart. Phys. 10 (2015) 015.

[17] J. Redondo, J. Cosmol. Astropart. Phys. 12 (2013) 008.

[18] K. Barth, A. Belov, B. Beltran, H. Bräuninger, J. M. Carmona, J. I. Collar, T. Dafni, M. Davenport, L. Di Lella, C. Eleftheriadis et al., J. Cosmol. Astropart. Phys. 05 (2013) 010.

[19] M. Archidiacono, S. Hannestad, A. Mirizzi, G. Raffelt, and Y. Y. Y. Wong, J. Cosmol. Astropart. Phys. 10 (2013) 020.

[20] G. G. Raffelt, in *Axions*, edited by M. Kuster, G. Raffelt, and B. Beltrán, Lecture Notes in Physics Vol. 741 (Springer-Verlag, Berlin, 2008), p. 51.

[21] J. E. Kim and G. Carosi, Rev. Mod. Phys. **82**, 557 (2010).

[22] F. Weber, *Pulsars as Astrophysical Laboratories for Nuclear and Particle Physics*, Studies in High Energy Physics, Cosmology and Gravitation (CRC Press, Boca Raton, 1999).

[23] A. Sedrakian, Prog. Part. Nucl. Phys. **58**, 168 (2007).

[24] D. Page, J. M. Lattimer, M. Prakash, and A. W. Steiner, arXiv:1302.6626.

[25] N. Iwamoto, Phys. Rev. Lett. **53**, 1198 (1984).

[26] N. Iwamoto, Phys. Rev. D **64**, 043002 (2001).

[27] M. Nakagawa, Y. Kohyama, and N. Itoh, Astrophys. J. **322**, 291 (1987).

[28] M. Nakagawa, T. Adachi, Y. Kohyama, and N. Itoh, Astrophys. J. **326**, 241 (1988).

[29] H. Umeda, N. Iwamoto, S. Tsuruta, L. Qin, and K. Nomoto, in *Neutron Stars and Pulsars: Thirty Years after the Discovery*, edited by N. Shibazaki (Universal Academy Press, Tokyo, 1998), p. 213.

[30] E. Flowers, M. Ruderman, and P. Sutherland, Astrophys. J. **205**, 541 (1976).

[31] A. V. Senatorov and D. N. Voskresensky, Phys. Lett. B **184**, 119 (1987).

[32] J. Keller and A. Sedrakian, Nucl. Phys. **A897**, 62 (2013).

[33] D. G. Yakovlev, A. D. Kaminker, and K. P. Levenfish, Astron. Astrophys. **343**, 650 (1999).

[34] L. B. Leinson and A. Pérez, Phys. Lett. B **638**, 114 (2006).

[35] A. Sedrakian, H. Müther, and P. Schuck, Phys. Rev. C **76**, 055805 (2007).

[36] E. E. Kolomeitsev and D. N. Voskresensky, Phys. Rev. C **77**, 065808 (2008).

[37] A. Sedrakian, Phys. Rev. C **86**, 025803 (2012).

[38] D. Page, J. M. Lattimer, M. Prakash, and A. W. Steiner, Astrophys. J. **707**, 1131 (2009).

[39] P. S. Shternin, D. G. Yakovlev, C. O. Heinke, W. C. G. Ho, and D. J. Patnaude, Mon. Not. R. Astron. Soc. **412**, L108 (2011).

[40] D. Blaschke, H. Grigorian, D. N. Voskresensky, and F. Weber, Phys. Rev. C **85**, 022802 (2012).

[41] H. A. Grigorian, D. B. Blaschke, and D. N. Voskresensky, J. Phys. Conf. Ser. **496**, 012014 (2014).

[42] D. Viganò, N. Rea, J. A. Pons, R. Perna, D. N. Aguilera, and J. A. Miralles, Mon. Not. R. Astron. Soc. **434**, 123 (2013).

[43] P. S. Shternin and D. G. Yakovlev, Mon. Not. R. Astron. Soc. **446**, 3621 (2015).

[44] D. Hess and A. Sedrakian, Phys. Rev. D **84**, 063015 (2011).

[45] A. Sedrakian, Astron. Astrophys. **555**, L10 (2013).

[46] A. Sedrakian, arXiv:1509.06986.

[47] S. M. de Carvalho, R. Negreiros, M. Orsaria, G. A. Contrera, F. Weber, and W. Spinella, Phys. Rev. C **92**, 035810 (2015).

[48] http://www.astroscu.unam.mx/neutrones/NSCool/. We use the equation of state input contained in the files `Crust-EOS-Cat-HZD-NV.dat`, `APR-EOS-Cat.dat`, and pairing gap inputs specified by `I-Pairing-SFB-b-T73.dat`.

[49] C. A. Baker, D. D. Doyle, P. Geltenbort, K. Green, M. G. D. van der Grinten, P. G. Harris, P. Iaydjiev, S. N. Ivanov, D. J. R. May, J. M. Pendlebury et al., Phys. Rev. Lett. **97**, 131801 (2006).

[50] M. V. Zverev, J. W. Clark, and V. A. Khodel, Nucl. Phys. **A720**, 20 (2003).

[51] A. D. Kaminker, C. J. Pethick, A. Y. Potekhin, V. Thorsson, and D. G. Yakovlev, Astron. Astrophys. **343**, 1009 (1999).

[52] D. G. Yakovlev and K. P. Levenfish, Astron. Astrophys. **297**, 717 (1995).

[53] E. V. Gotthelf, J. P. Halpern, and J. Alford, Astrophys. J. **765**, 58 (2013).

[54] K. G. Elshamouty, C. O. Heinke, G. R. Sivakoff, W. C. G. Ho, P. S. Shternin, D. G. Yakovlev, D. J. Patnaude, and L. David, Astrophys. J. **777**, 22 (2013).

[55] A. De Luca, P. A. Caraveo, S. Mereghetti, M. Negroni, and G. F. Bignami, Astrophys. J. **623**, 1051 (2005).